

Biodegradable Polylactide/Montmorillonite Nanocomposites

Suprakas Sinha Ray,^{a,*} Kazunobu Yamada,^b Masami Okamoto,^{a,*} and Kazue Ueda^b

^aAdvanced Polymeric Materials Engineering, Graduate School of Engineering, Toyota Technological Institute, Nagoya 468 851, Japan

^bUnitika Ltd., Kyoto 611 0021, Japan

Our continuing research on the preparation, characterization, materials properties, and biodegradability of polylactide (PLA)/organically modified layered silicate (OMLS) nanocomposites has yielded results on PLA/montmorillonite nanocomposites. Montmorillonite (mmt) modified with dimethyldioctadecylammonium cation was used as an OMLS for nanocomposite preparation. The internal structure of nanocomposites on the nanometer scale was established with the use of wide-angle X-ray diffraction patterns and transmission electron micrographic observation. All nanocomposites exhibited significant improvement in crystallization behavior, mechanical properties, flexural properties, heat distortion temperature, and O₂ gas permeability when compared with pure PLA.

Keywords: Polylactide, Montmorillonite, Nanocomposite, Crystallization, Materials Properties.

1. INTRODUCTION

Over the last few years, polymer/layered silicate nanocomposites have attracted great interest from researchers, both in industry and in academia, because they often exhibit remarkable improvement of materials properties when compared with pure polymer or conventional composites (both micro- and macro-composites). These improvements include higher moduli,¹ increased strength and heat resistance,² decreased gas permeability³ and flammability,⁴ and increased biodegradability of biodegradable polymers.⁵ On the other hand, these materials have also been proved to be unique model systems for the study of the structure and dynamics of polymers in confined environments.⁶

The commonly used layered silicates for the preparation of polymer/layered silicate nanocomposites belong to the same general family of 2:1 layered or phyllosilicates.⁷ Their crystal structure consists of layers made up of two silica tetrahedra fused to an edge-shared octahedral sheet of either aluminum or magnesium hydroxide. The layer thickness is around 1 nm, and the lateral dimensions of these layers may vary from 30 nm to several micrometers and even larger, depending on the particular layered silicate. Stacking of the layers leads to a regular van der Waals gap between the layers called the *interlayer* or *gallery*. Isomorphic substitution within the layers (for example, Al³⁺ replaced by Mg²⁺ or by Fe²⁺, or Mg²⁺ replaced by Li⁺) generates negative charges that are counterbalanced by alkali and alkaline earth cations situated inside the galleries. The type of layered silicate is characterized by a moderate surface charge (known as cation exchange capacity (CEC), and generally expressed

in mequiv/100 g). This charge is not locally constant, as it varies from layer to layer and must rather be considered as an average value over the whole crystal. Layered silicates have two types of structure, tetrahedral-substituted and octahedral-substituted. In case of tetrahedral-substituted layered silicates the negative charge is located on the surface of silicate layers, and, hence, the polymer matrices can react with tetrahedral-substituted silicate more compared with that of octahedral-substituted.⁷

Pristine layered silicates usually contain hydrated Na⁺ or K⁺ ions.⁸ Obviously, in this pristine state layered silicates are only miscible with hydrophilic polymers, such as poly(ethylene oxide) (PEO),⁹ poly(vinyl alcohol) (PVA),¹⁰ etc. To render layered silicates miscible with other polymer matrices, one must convert the normally hydrophilic silicate surface to organophilic, which makes possible the intercalation of many engineering polymers. Generally, this can be done by ion-exchange reactions with cationic surfactants, including primary, secondary, tertiary, and quaternary alkylammonium or alkylphosphonium cations. The role of alkylammonium or alkylphosphonium cations in the organosilicates is to lower the surface energy of the inorganic host and to improve the wetting characteristics with the polymer matrix; this results in a larger interlayer spacing. Additionally, the alkylammonium or alkylphosphonium cations could provide functional groups that can react with the polymer matrix or in some cases initiate the polymerization of monomers to improve the strength of the interface between the inorganic and the polymer matrix.^{11, 12}

The main reason for the improved properties of pure polymer in nanocomposites is interfacial interaction between polymer matrix and organically modified layered silicate (OMLS) as opposed to conventional composites. A few

*Authors to whom correspondence should be addressed.

weight percent of OMLS that is properly dispersed throughout the matrix thus creates a much higher surface area for polymer-filler interfacial interactions than do conventional composites.¹³ On the basis of the strength of polymer-OMLS interactions, three different types of nanocomposites are structurally achievable: *intercalated nanocomposites*, where insertion of polymer chains into the layered silicate structure occurs in a crystallographically regular fashion, regardless of the polymer-to-OMLS ratio, and a repeat distance of few nanometers; *flocculated nanocomposites*, where intercalated stacked silicate layers eventually flocculate because of the hydroxylated edge-edge interactions; and *exfoliated nanocomposites*, where the individual silicate layers are separated in a polymer matrix by average distances that totally depend on the clay loading.¹⁴

Recently, the development of biodegradable polymeric materials with excellent materials properties is a subject of great research challenge in materials science. One of the most promising polymers in this direction is polylactide (PLA) because it is made from renewable agriculture products and is readily biodegradable.^{15, 16} PLA is linear aliphatic thermoplastic polyester, produced by the ring-opening polymerization of lactide.^{17–19} Lactide is a cyclic dimer prepared by the controlled depolymerization of lactic acid, which in turn is obtained by the fermentation of corn, sugar beet, etc.^{15, 16} It has very good mechanical properties, thermal plasticity, fabric ability, and biocompatibility.^{20–21} Even when burned it produces no nitrogen oxide gases and only one-third the combustible heat generated by polyolefin, and does not damage incinerators and, thus, provides significant energy savings.²² So PLA is a promising polymer for various end-use applications, and currently there is increasing interest in using PLA for disposable degradable plastic articles.²³ However, some other properties such as heat distortion temperature (HDT), flexural and gas barrier properties, and melt viscosity for further processing are frequently not good enough for wide-ranging applications.²⁴ On the other hand, preparation of nanocomposites with OMLS has already proved to be an effective way to improve these properties significantly.^{1–6}

In our previous papers,^{25–29} we have reported on the preparation, characterization, and materials properties of various kinds of PLA/OMLS nanocomposites. In this paper we describe the preparation, characterization, crystallization behavior, mechanical and material properties of another type of PLA nanocomposite prepared with dimethyldioctadecylammonium-modified montmorillonite with a simple melt extrusion technique.

2. EXPERIMENTAL DETAILS

2.1. Materials

PLA with *D* content of 1.1–1.7% (supplied by Unitika Co. Ltd., Japan) was dried under vacuum at 60 °C and kept under dry nitrogen gas for 1 week prior to use. The organ-

ically modified montmorillonite ($C^2C^2_{18}$ -mmt) used in this study was supplied by Hojun Yoka Co., Japan, and was synthesized by replacing Na^+ in montmorillonite (mmt) (original thickness of ~ 1 nm and average length of 100 nm) of a CEC of 90 mequiv/100 g with dimethyldioctadecylammonium cation by ion exchange reaction.

2.2. Nanocomposite Preparation

For nanocomposite preparation, $C^2C^2_{18}$ -mmt (powder form) and PLA (pellet form) were first dry-mixed by shaking them in a bag. The mixture was then melt-extruded with a twin-screw extruder (PCM-30, Ikegai machinery Co.) operated at 210 °C³⁰ (screw speed = 100 rpm, feed rate = 120 g/min) to yield nanocomposite strands. Henceforth, the product nanocomposites are abbreviated as PLACNs. PLACNs prepared with three different amounts of $C^2C^2_{18}$ -mmt of 4, 5, and 7 wt% are correspondingly abbreviated as PLACN4, PLACN5, and PLACN7, respectively. The strands were pelletized and dried under vacuum at 60 °C for 48 h to remove water.

The dried PLACN pellets were then converted into sheets with a thickness of 0.7–2 mm by pressing with ~ 1.5 MPa at 190 °C for 3 min. The molded sheets were then quickly quenched between glass plates and then annealed at 110 °C for 1.5 h to crystallize isothermally before being subjected to wide-angle X-ray diffraction (WAXD), transmission electron microscopy (TEM), and dynamic mechanical property measurements.

2.3. Characterization

2.3.1. WAXD

WAXD analyses were performed for the $C^2C^2_{18}$ -mmt powder and three different PLACN sheets with an MXlabo X-ray diffractometer (MAC Science Co., generator of 3 kW, a graphite monochromator, CuK_{α} radiation (wavelength, $\lambda = 0.154$ nm), operated at 40 kV/20 mA). The samples were scanned in fixed-time (FT) mode with a counting time of 2 s under a diffraction angle of 2θ in the range of 1° to 70°.

2.3.2. TEM

To clarify the nanoscale structure of various PLACNs, high-resolution TEM (H-7100; Hitachi Co.) was also used, at an accelerating voltage of 100 kV. An ultrathin section of crystallized sheet (perpendicular to the compression mold) with a thickness of ~ 100 nm was microtomed at -80 °C with a Reichert Ultra cut cryo-ultramicrotome without staining.

2.3.3. Gel Permeation Chromatography

Weight-averaged (M_w) and number-averaged (M_n) molecular weights of PLA (before and after nanocomposite

preparation) were determined by gel permeation chromatography (GPC) (LC-VP, Shimadzu Co.), with polystyrene standards for calibration and tetrahydrofuran (THF) as the carrier solvent at 40 °C, with a flow rate of 0.5 ml/min. For the GPC measurements first PLA or nanocomposites were dissolved in CHCl_3 and then diluted with THF. In the case of nanocomposites, after dissolving in CHCl_3 the insoluble clay particles were separated from the dissolved PLA by filtration.

2.3.4. Differential Scanning Calorimetry

The glass transition (T_g), melting (T_m), and crystallization (T_c) temperatures, as well as degree of crystallinity (χ_c) of pure PLA and PLACNs, were determined by temperature-modulated differential scanning calorimetry (DSC) (TMDSC) (MDSC, TA2920, TA instruments), operated at a heating rate of 5 °C/min with a heating/cooling cycle of the modulation period of 60 s and an amplitude of ± 0.769 °C. For the measurement of χ_c prior to DSC analysis, the extra heat absorbed by the crystallites formed during heating had to be subtracted from the total endothermic heat flow due to the melting of the whole crystallites. This can be done according to the principles and procedures described in our previous paper.³¹ By considering the melting enthalpy of 100% crystalline poly(L-lactide) as 93 J/g,³² we have estimated the value of the χ_c for pure PLA and PLACNs, which is presented in Table I.

2.3.5. Light Scattering and Polar Optical Micrographic Observations

To investigate the crystallite texture, the pure PLA and PLACN samples were subjected to light scattering (LS) experiments under Hv scattering mode with the radiation of a polarized He-Ne laser at 632.8-nm wavelength. The details of the LS measurement were described in our previous paper.³³

We also observed the crystallite growth behavior of pure PLA and PLACNs with a polar optical micrograph (POM). Dried pellets were sandwiched between two glass slides

and placed on a laboratory hot plate at 200 °C for 60 s to obtain a thin film ~ 30 μm in thickness. The molten film was then quickly quenched to the desired temperature (100 °C) by putting it on a thermostatted hot stage (Linkam RTVMS; Linkam Scientific Instruments, Ltd.) mounted on a POM (Nikon OPTIPHOTO2-POL). After complete crystallization, the nature of crystallite growth was observed with a POM.

2.3.6. Dynamic Mechanical Analysis

Dynamic mechanical properties of the pure PLA and PLACNs were measured with a Reometrics Dynamic Analyzer (RDAlI) in the tension-torsion mode. The temperature dependence of dynamic storage modulus (G'), loss modulus (G''), and their ratio, $\tan \delta$, of pure PLA and various PLACNs were determined at a constant frequency (ω) of 6.28 rad/s with a strain amplitude of 0.05%, and in the temperature range of -20 to 160 °C with a heating rate of 2 °C/min.

2.3.7. Flexural Properties and Heat Distortion Temperature

The sample pellets were injection-molded with an injection machine (IS-80G; Toshiba Machinery Co.) operated at 190 °C with a mold temperature of 30 °C. Flexural modulus and strength of the injection-molded specimens (thickness ~ 3.2 mm, annealed at 120 °C for 30 min) were measured according to the ASTM D-790 method (model 2020; Intesco Co.) with a strain rate of 2 mm/min at room temperature (~ 25 °C). The heat distortion temperature (HDT) tests of neat PLA and various PLACNs were conducted with crystallized injection molded samples (HDT Tester; Toyoseiki Co.) according to the ASTM D-648 method with a heating rate of 2 °C/min. We also conducted load dependence of HDT of neat PLA and PLACN7 by the same procedure.

2.3.8. Measurement of O_2 Gas Transmission Rates

Oxygen gas transmission rates of pure PLA and various PLACNs were measured at 20 °C and 90% relative humidity by the ASTM D-1434 differential pressure method (GTR-30XAU; Yanaco Co.). Test samples were prepared by compression molding (thickness ~ 300 μm), and melt-quenched samples were used for this measurement.

Table I. Characteristic parameters of neat PLA and various PLACNs.

Parameters	Neat PLA	PLACN4	PLACN5	PLACN7
$M_w \times 10^{-3}$ (g·mol ⁻¹)	177 ^a	163	158	155
M_w/M_n	1.58	1.61	1.60	1.59
T_g (°C)	60	58.6	57.4	57.3
T_m (°C)	168	170	169.6	169.6
T_c (°C)	127.2	101	101.7	100.6
χ_c (%)	36	47.5	47.2	51.7
$N \times 10^5$ (μm^{-3})	2.7	822.6	337.4	207.9
d_{001} (nm)	—	3	2.95	2.85
D (nm) ^b	—	11.3	14.5	15.9
D/d_{001}	—	4	5	6

^aExtruded PLA under the same condition.

^bCalculated by using Scherrer equation.

3. RESULTS AND DISCUSSION

3.1. Nanocomposite Structure

The structure of the nanocomposites in the nanometer range has typically been elucidated by WAXD and TEM. WAXD provides direct evidence of the intercalation of the polymer chains into the silicate galleries. On the other

hand, TEM offers a qualitative understanding of the internal structure through direct visualization. WAXD patterns for the pure $C^2C^2_{18}$ -mmt powder and three different PLACNs are presented in Figure 1. The interlayer gallery height, calculated as the difference of the d_{001} distances obtained by WAXD and the individual layer thickness for the $C^2C^2_{18}$ -mmt, is 2.5 nm, which, upon intercalation by PLA, expands to ~ 3 nm in the case of PLACN4. With increasing clay content this distance gradually decreases, and the value of d_{001} is equal to 2.85 nm in the case of PLACN7. From the WAXD patterns, the crystallite size (D) of intercalated stacked silicate layers of each PLACN is calculated with the Scherrer equation.³⁴ The calculated value of D for each PLACN is also presented in Table I. It is clearly established that the crystallite size (the thickness of the dispersed stacked silicate layers) in the PLACNs

gradually increases with increasing clay loading. Therefore, we can conclude that the well-ordered intercalated PLACNs were formed and coherence order of the silicate layers increases with increasing $C^2C^2_{18}$ -mmt content. Dividing the value of D by the d_{001} value of each PLACN, we can estimate the number of the stacked individual silicate layers to be about 4 for PLACN4, 5 for PLACN5, and about 6 in the case of PLACN7.

On the other hand, TEM is a qualitative tool used for the determination of overall clay dispersion. Figure 2 shows the typical bright-field TEM image of PLACN5 in which dark entities are the cross section of the stacked and intercalated silicate layers.³⁵ From the TEM image, we observed the large anisotropy of the stacked and flocculated silicate layers, which have an original thickness of ~ 1 nm and an average length of ~ 100 nm.

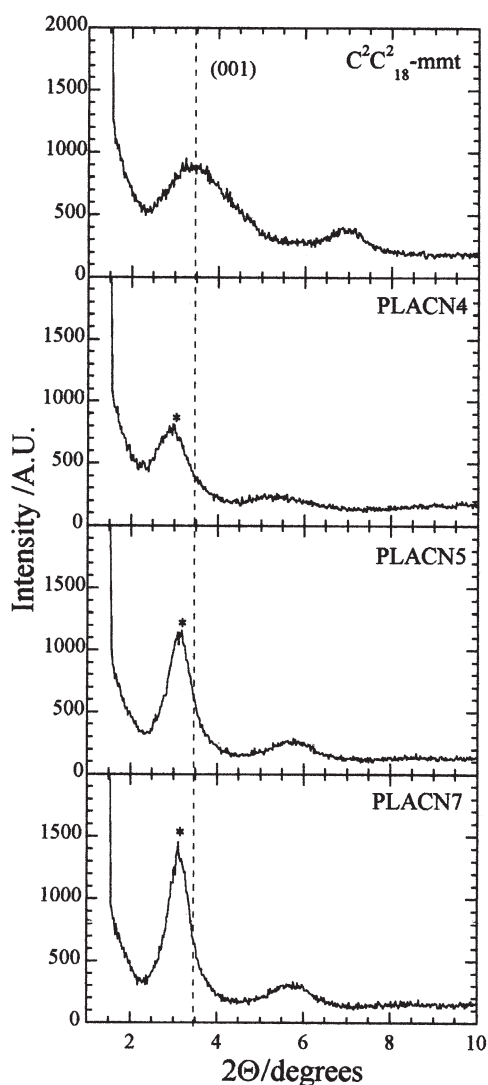


Fig. 1. WAXD patterns of $C^2C^2_{18}$ -mmt powder and various PLACNs. The dashed line indicates the location of the silicate (001) reflection of $C^2C^2_{18}$ -mmt. The asterisks indicate the (001) peak for $C^2C^2_{18}$ -mmt dispersed in PLA matrix.

3.2. GPC

GPC results of PLA in the pure state or in $C^2C^2_{18}$ -mmt-filled systems are also presented in Table I. As anticipated, the incorporation of $C^2C^2_{18}$ -mmt resulted in a reduction in the molecular weight of the PLA matrix. Decreased molecular weights of PLA in nanocomposites may be explained by the shear mixing of PLA and $C^2C^2_{18}$ -mmt, resulting in a certain extent of hydrolysis of PLA matrix at high temperature.

3.3. Thermal Properties and Crystallite Morphology

Figure 3 shows DSC traces for the melt-quenched samples of neat PLA and three different PLACNs. These data are obtained from the first run and during the heating process. Samples were prepared by using a hot press. Neat PLA and PLACN pellets were melted at 190 °C hold for 3 min

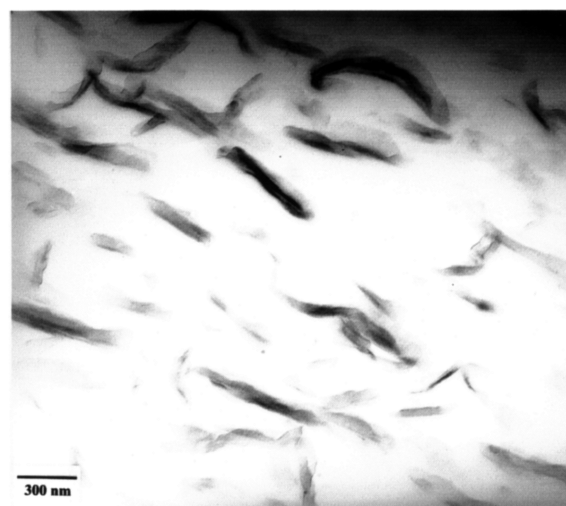


Fig. 2. High-resolution TEM bright-field image of crystallized PLACN5 sheet. The dark entities are the cross section of the intercalated mmt layers, and the bright areas are the matrix.

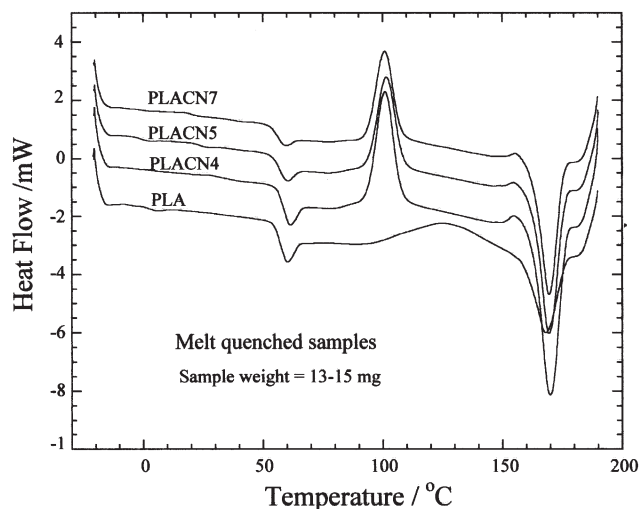


Fig. 3. DSC scans of the melt-quenched samples of pure PLA and various PLACNs.

at the same temperature under ~ 1.5 MPa pressure, and then quickly quenched between glass plates. From Figure 3 we can see an endothermic peak for all samples in the temperature range of 55–60 °C. The temperature corresponding to the endothermic peak for each sample is considered to be T_g of PLA. For all samples at T_g there is a steplike change, which is due to enthalpy relaxation. This type of steplike change at T_g has also been recognized for some other polymers.³⁶

On the other hand, all samples show an exothermic peak, and that can be correlated to the crystallization of PLA in every sample; the corresponding temperature is known as the crystallization temperature, T_c . In the case of PLACNs this peak is sharper and appeared at lower temperature than that of neat PLA (see Table I). Therefore, $C^2C^2_{18}$ -mmt seems to enhance the rate of crystallization of PLA. It should be noted here that T_c does not depend upon $C^2_{18}C^2$ -mmt. This behavior suggests that a small amount of $C^2C^2_{18}$ -mmt is enough to serve as a nucleating agent for crystallization. A systematic DSC study of all samples shows that the T_g signal of neat PLA gradually weakens with increasing $C^2C^2_{18}$ -mmt content. This behavior suggests that $C^2C^2_{18}$ -mmt layers affect all polymers, and there is very small amount of bulk-like PLA present to manifest itself through the thermal transition.

POM photographs of neat PLA and various PLACNs are presented in Figure 4a. All samples were crystallized at 100 °C beforehand. Neat PLA exhibits well-defined large crystallite morphology, whereas the size of the PLACN crystallites is significantly smaller. This observation indicates that the surface of dispersed $C^2C^2_{18}$ -mmt has a very strong effect on PLA crystallization.

This behavior is more clearly seen in LS patterns (see Fig. 4b), where, for PLACNs, a clear large smeared four-leaf-clover pattern is observed compared with the crystallized neat PLA, indicating formation of a large number of

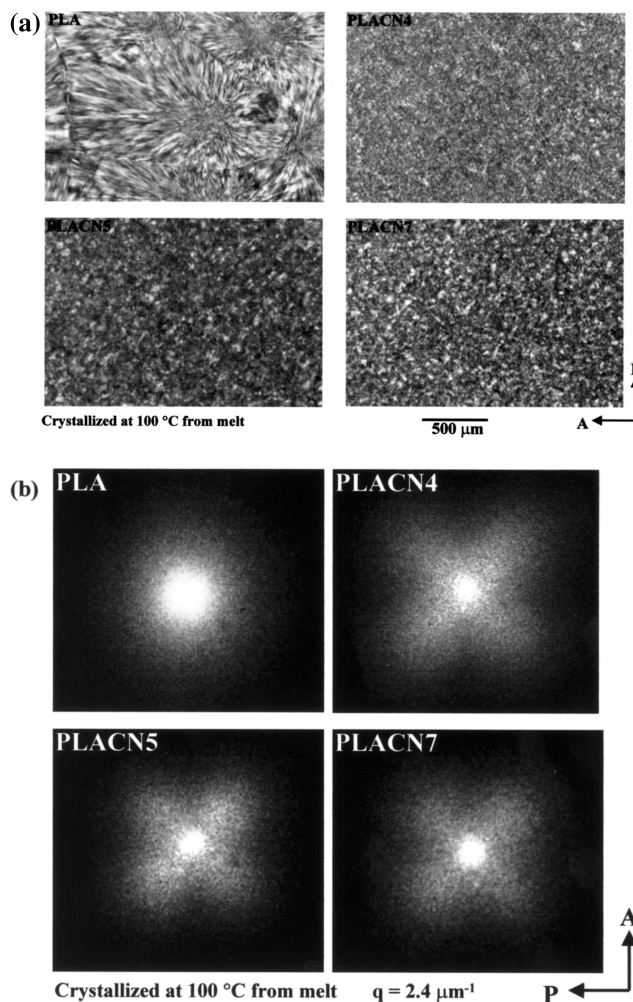


Fig. 4. (a) Polarized optical micrographs of pure PLA and various PLACNs isothermally crystallized at 100 °C for 1.5 h. (b) Hv-light scattering patterns for pure PLA and various PLACNs isothermally crystallized at 110 °C for 1.5 h.

less organized crystallites. From LS patterns, the number of heterogeneous nuclei N can be estimated from a rough approximation (i.e., all of the crystallites are of identical size). The primary average nucleation density of the crystallites, N , is given by³⁷

$$N = (3/4\pi)(D_m/2)^{-3}$$

where D_m is the average maximum diameter of the crystallite, that is, the attainable diameter before impingement. The calculated values of N at 100 °C are also presented in Table I. This behavior indicates that the surface of the dispersed $C^2C^2_{18}$ -mmt layers acts as a nucleating agent for PLA crystallization, which is evident from the increase in the number of density of nuclei causing smaller crystallite formation.³⁷ So our investigation explores the role of $C^2C^2_{18}$ -mmt as a nucleating agent for PLA crystallization. Such a discussion is beyond the objective of this paper, and we will report it separately.³⁸

3.4. DMA

DMA measures the response of a given material to an oscillatory deformation (here in tension-torsion mode) as a function of the temperature. DMA results are expressed by three main parameters: (a) the storage modulus (G'), corresponding to the elastic response to the deformation; (b) the loss modulus (G''), corresponding to the plastic response to the deformation, and (c) $\tan \delta$, that is, the G''/G' ratio, which is useful for determining the occurrence of molecular mobility transitions such as the glass transition temperature.

Here DMA analysis has been studied to track the temperature dependence of storage modulus upon PLACN formation. Figure 5 shows the temperature dependence of G' , G'' , and $\tan \delta$ for PLA and corresponding PLACNs. For all PLACNs, significant enhancement of G' can be seen in the investigated temperature range, indicating that intercalated PLACN is strongly influenced by the elastic properties of the PLA matrix.

Below T_g , the enhancement of G' is clear in the intercalated PLACNs, but at the temperature range of 80 °C to 145 °C all three nanocomposites exhibit much higher enhancement of G' as compared with that of pure PLA. This is due to the mechanistic reinforcement by clay particles at high temperature. Above T_g , when materials become soft, the reinforcement effect of the clay particles becomes

prominent and hence a strong enhancement of the modulus appears.^{14, 39}

On the other hand, above T_g the enhancement of G'' is significant in the intercalated PLACNs in comparison with that below T_g , indicating a plastic response to the deformation is prominent in the presence of clay when material becomes soft. However, the presence of clay particles does not lead to a significant shift and broadening of the $\tan \delta$ curves for all PLACNs compared with that of pure PLA. This behavior has been ascribed to the restricted segmental motions at the organic–inorganic interface neighborhood of intercalated PLACNs.

3.5. Flexural Properties and HDT

In Table II, we report the flexural modulus, flexural strength, and distortion at break of neat PLA and three PLACNs measured at 25 °C. There is a significant increase of flexural modulus for PLACN4 compared with that of pure PLA followed by a constant value with increasing $C^2C^2_{18}$ -mmt content. On the other hand, flexural strength and distortion at break exhibited a remarkable increase with PLACN4 and then gradually decreased with $C^2C^2_{18}$ -mmt loading. This behavior may be due to the high $C^2C^2_{18}$ -mmt content, which leads to a brittleness of materials. Therefore, we can control the flexural strength and distortion by increasing or decreasing OMLS content, and incorporation of $C^2C^2_{18}$ -mmt of around 4 wt% is the optimum for achieving a high value of flexural strength and distortion.

The nanodispersion of $C^2C^2_{18}$ -mmt in pure PLA also promotes a higher HDT. We examined the HDT of pure PLA and various PLACNs with different load conditions. As seen in Figure 6a, in the case of PLACN4, there is a marked increase in HDT with an intermediate load of 0.98 MPa, from 76 °C for the pure PLA to 91.3 °C for PLACN4. The value of HDT gradually increases with increasing clay content, and, in the case of PLACN7, the value increases to 107 °C.

On the other hand, imposed load dependence on HDT is clearly observed in the case of PLACNs. Figure 6b shows the typical load dependence in the case of PLACN7. The increase in HDT of neat PLA due to nanocomposite preparation is a very important property improvement, not only from the industrial point of view but also for molecular control on the silicate layers, that is, crystallization through interaction between PLA molecules and SiO_4 tetrahedral layers.

In the case of high load (1.81 MPa), it is very difficult to achieve high HDT enhancement without strong interaction

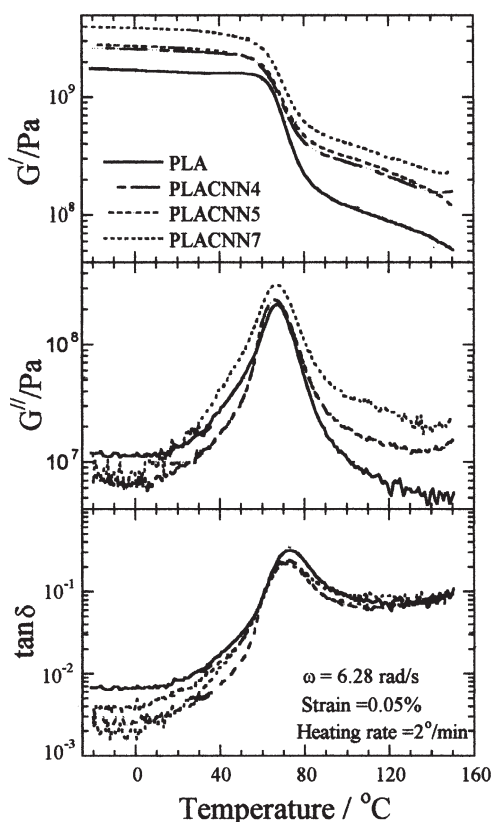


Fig. 5. Temperature dependence of storage modulus (G'), loss modulus (G''), and their ratio, $\tan \delta$, for pure PLA and various PLACNs.

Table II. Flexural properties of neat PLA and various PLACNs.

Flexural properties	Neat PLA	PLACN4	PLACN5	PLACN7
Modulus (GPa)	4.84	5.43	5.38	5.39
Strength (MPa)	86	102	107	99
Distortion (%)	1.9	3.9	2.1	1.9

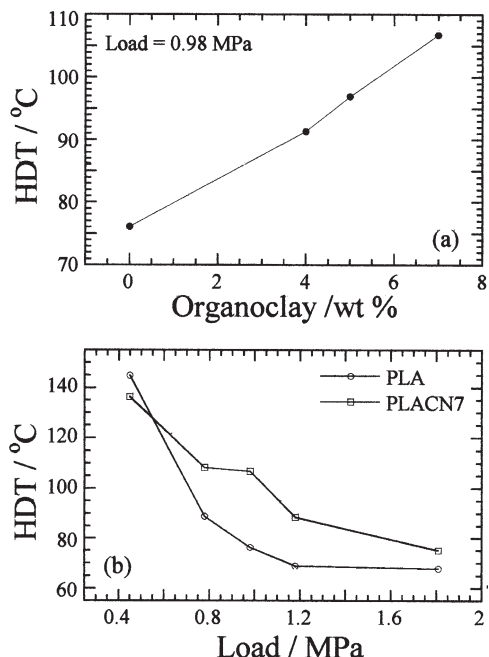


Fig. 6. (a) Organoclay ($C^{2}C^{2}_{18}$ -mmt) (wt%) dependence of HDT of pure PLA and various PLACNs. (b) Load dependence of HDT of pure PLA and PLACN7.

between polymer matrix and OMLS.⁴⁰ In the case of all PLACNs studied here, the values of T_m (cf. Table I) do not change significantly as compared with that of pure PLA. Furthermore, in WAXD analyses up to $2\theta = 70^\circ$ (see Fig. 7), we observed no big shift or formation of new peaks in the crystallized PLACNs. So the improvement of HDT with intermediate load (0.98 MPa) originates from the better mechanical stability of the PLACNs due to mechanical reinforcement by the dispersed clay particles, higher value of χ_c , and intercalation. This is qualitatively different from the behavior of nylon-6/OMLS nanocomposites, where the mmt layers stabilize in a crystalline phase different from that found in the neat nylon-6, with a higher HDT.⁴¹

3.6. Oxygen Gas Permeability

Nanoclays are believed to increase the gas barrier properties by creating a maze or “tortuous path” that retards the progress of gas molecules through the matrix resin.^{3, 42, 43} The mechanism for the improvement is attributed to the increase in the tortuosity of the diffusive path for a penetrating molecule. Indeed, a simple tortuosity-based model has been found to explain experimental trends satisfactorily. The gas permeability of nanocomposites (P_{PLACN}) is related to the permeability of the pure PLA (P_{PLA}) and the volume fraction (ϕ_{clay}) and width (D_{clay}) of the dispersed clay as⁴⁴

$$\frac{P_{PLACN}}{P_{PLA}} = \frac{1}{1 + (L_{clay}/2D_{clay})\phi_{clay}}$$

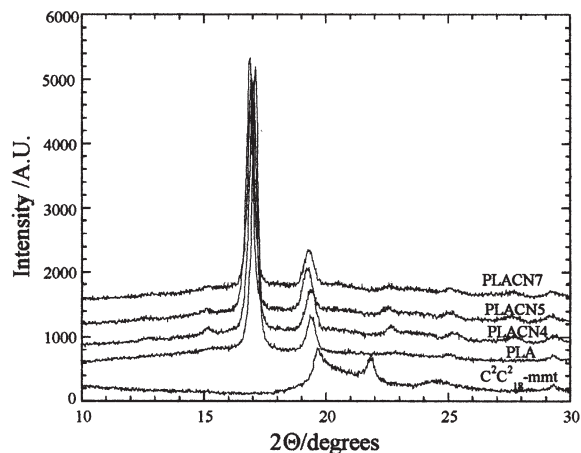


Fig. 7. WAXD patterns of pure PLA and various PLACNs. Samples were crystallized at 110 °C for 1.5 h before measurements. The data were vertically offset to make a clear presentation.

The above expression assumes that the sheets are placed such that the sheet plane is perpendicular to the diffusive pathway. The O_2 gas permeability for the pure PLA and various PLACNs are presented in Figure 8. As seen from Figure 8, the permeability of O_2 gas through the PLACN films improved compared with pure PLA film.

4. CONCLUSIONS

We have successfully prepared biodegradable polylactide/ $C^{2}C^{2}_{18}$ -mmt nanocomposites by simple melt extrusion of PLA and $C^{2}C^{2}_{18}$ -mmt, wherein silicates of $C^{2}C^{2}_{18}$ -mmt are intercalated, stacked and flocculated, and nicely distributed in the PLA matrix. All nanocomposites exhibited significant improvement in mechanical and various other materials properties when compared with those of neat PLA. These improvements include rate of crystallization, mechanical and flexural properties, heat distortion temperature, and O_2 gas permeability. These concurrent property improvements are well beyond what can be generally

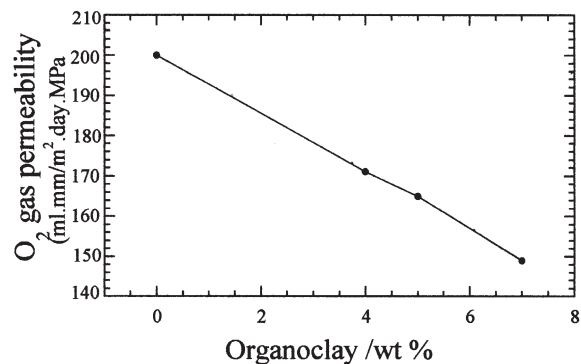


Fig. 8. Oxygen gas permeability of pure PLA and various PLACN films as a function of organoclay ($C^{2}C^{2}_{18}$ -mmt) content (wt%) measured at 20 °C and 90% relative humidity.

achieved through the micro/macro-composite preparation or chemical modification of pure PLA.

Acknowledgment: Thanks are due to the Japan Society for the Promotion of Science (JSPS) for the award of a postdoctoral fellowship and a research grant to S.S.R. (no. P02152).

References and Notes

- M. Biswas and S. Sinha Ray, *Adv. Polym. Sci.* 155, 167 (2001); M. Alexander and P. Dubois, *Mater. Sci. Eng.* R28, 1 (2000).
- E. P. Giannelis, *Appl. Organomet. Chem.* 12, 675 (1998).
- P. B. Messersmith and E. P. Giannelis, *J. Polym. Sci. Part A: Polym. Chem.* 33, 1047 (1995); K. Yano, A. Usuki, A. Okada, T. Kurauchi, and O. Kamogaito, *J. Polym. Sci. Part A: Polym. Chem.* 31, 2493 (1993).
- J. W. Gilman, *Appl. Clay Sci.* 15, 31 (1999).
- S. Sinha Ray, K. Yamada, M. Okamoto, and K. Ueda, *NanoLetters* 2, 1093 (2002); S. Sinha Ray, K. Yamada, M. Okamoto, and K. Ueda, *Macromol. Mater. Eng.* 288, 203 (2003).
- R. A. Vaia, K. D. Jandt, E. J. Kramer, and E. P. Giannelis, *Macromolecules* 28, 8080 (1995).
- S. Sinha Ray and M. Okamoto, *Prog. Polym. Sci.*, in press.
- S. W. Brindly and G. Brown, editors, *Crystal Structure of Clay Minerals and Their X-ray Diffraction*, Mineralogical Society, London (1980).
- P. Aranda and E. Ruiz-Hitzky, *Chem. Mater.* 4, 1395 (1992).
- D. J. Greenland, *J. Colloid. Sci.* 18, 647 (1963).
- A. Blumstein, *J. Polym. Sci. A* 3, 2665 (1965).
- R. Krishnamoorti, R. A. Vaia, and E. P. Giannelis, *Chem. Mater.* 8, 1728 (1996).
- J. S. Chen, M. D. Poliks, C. K. Ober, Y. Zhang, U. Wiesner, and E. P. Giannelis, *Polymer* 43, 4895 (2002).
- S. Sinha Ray, K. Okamoto, and M. Okamoto, *Macromolecules* 36, 2355 (2003).
- R. E. Drumright, P. R. Gruber, and D. E. Henton, *Adv. Mater.* 12, 1841 (2000).
- J. Lunt, *Polym. Degrad. Stab.* 59, 145 (1998).
- S. H. Kim, Y. K. Han, Y. H. Kim, and S. I. Hong, *Macromol. Chem.* 193, 1623 (1991); H. R. Kricheldorf and A. Serra, *Polym. Bull.* 14, 497 (1985).
- H. R. Kricheldorf, M. Berl, and N. Scharngal, *Macromolecules* 21, 286 (1988).
- A. J. Nijenhuis, D. W. Grijpma, and A. J. Pennings, *Macromolecules* 25, 6419 (1992).
- O. Martin and L. Averous, *Polymer* 42, 6209 (2001); H. Tsuji and Y. Ikada, *J. Appl. Polym. Sci.* 67, 405 (1998).
- Q. Fang and M. A. Hanna, *Ind. Crops Prod.* 10, 47 (1999).
- From Kanebo Ltd., Japan, wave site www.kanebotx.com (accessed Aug. 27, 2002).
- J. D. Gu, M. Gada, G. Kharas, D. Eberiel, S. P. McCarthy, and R. A. Gross, *Polym. Mater. Sci. Eng.* 67, 351 (1992).
- N. Ogata, G. Jimenez, H. Kawai, and T. Ogihara, *J. Polym. Sci. Part B: Polym. Phys.* 35, 389 (1997).
- S. Sinha Ray, K. Okamoto, K. Yamada, and M. Okamoto, *NanoLetters* 2, 423 (2002); S. Sinha Ray, P. Maiti, M. Okamoto, K. Yamada, and K. Ueda, *Macromolecules* 35, 3104 (2002).
- S. Sinha Ray, K. Yamada, A. Ogami, M. Okamoto, and K. Ueda, *Macromol. Rapid Commun.* 23, 943 (2002); S. Sinha Ray, K. Yamada, M. Okamoto, A. Ogami, and K. Ueda, *Chem. Mater.* 15, 1456 (2003).
- S. Sinha Ray, K. Yamada, M. Okamoto, and K. Ueda, *Polymer* 44, 857 (2003).
- S. Sinha Ray, K. Yamada, M. Okamoto, Y. Fujimoto, A. Ogami, and K. Ueda, *Polymer*, in press.
- S. Sinha Ray, M. Okamoto, K. Yamada, A. Ogami, and K. Ueda, *Macromolecules*, in press.
- We have checked the degradation of intercalated salt by using thermogravimetric (TG) analysis. Up to 210 °C, there is no degradation of intercalated salt.
- P. H. Nam, P. Maiti, M. Okamoto, T. Kotaka, N. Hasegawa, and A. Usuki, *Polymer* 42, 9633 (2001).
- E. W. Fisher, H. J. Sterzel, and G. Wegner, *Kolloid Z. Z. Polym.* 25, 980 (1973).
- M. Okamoto, H. Kubo, and T. Kotaka, *Macromolecules* 31, 4223 (1998).
- $D = (\lambda k)/(\beta \cos \theta)$, where k is a constant and generally equal to 0.9, $\lambda = 0.154$ nm, and θ is the WAXD peak position. B. D. Cullity, *Principles of X-ray Diffraction*, Addison-Wesley, Reading, MA (1978).
- Because the silicate layers are composed of heavier elements (Al, Si, O) than the interlayer and surrounding matrix (C, H, N, etc.), they appear darker in bright-field images. R. E. Klimentidis and I. D. R. Mackinnon, *Clays Clay Miner.* 34, 155 (1986).
- B. Wunderlich, *Macromolecular Physics*, Academic Press, New York (1976), Vol. 2, p. 363.
- P. Maiti, P. H. Nam, M. Okamoto, A. Usuki, and N. Hasegawa, *Macromolecules* 35, 2042 (2002), and references cited therein.
- J. Y. Nam, S. Sinha Ray, and M. Okamoto, *Macromolecules*, in press.
- S. Sinha Ray, K. Okamoto, P. Maiti, and M. Okamoto, *J. Nanosci. Nanotechnol.* 2, 171 (2002).
- A. Usuki, M. Kawasumi, Y. Kojima, A. Okada, T. Kurauchi, and O. Kamigaito, *J. Mater. Res.* 8, 1185 (1993).
- E. Manias, A. Touny, L. Wu, K. Strawhecker, B. Lu, and T. C. Chung, *Chem. Mater.* 13, 3516 (2001).
- S. Sinha Ray, K. Yamada, M. Okamoto, and K. Ueda, *Comp. Interfaces*, in press.
- G. W. Beall, in *Polymer-Clay Nanocomposites*, edited by T. J. Pinnavaia and G. W. Beall, Wiley, New York, (2001), p. 267.
- L. Nielsen, *J. Macromol. Sci. Chem.* A1(5), 929 (1967).

Received: 11 April 2003. Revised/Accepted: 1 May 2003.

[Author:
Need
updates
for Refs.
7, 28, 29,
38, and
42.]